Environmental Earth Sciences (2023) 82:373
https://doi.org/10.1007/s12665-023-11036-5

ORIGINAL ARTICLE

The potential influence of drains on the recent sediment characteristics and sedimentation rates of Lake Qarun, Western Desert, Egypt

Noha Imam[1] · **Salem Ghonamy Salem**[2]

Received: 4 February 2023 / Accepted: 24 June 2023

Abstract
In recent decades, Lake Qarun significantly suffered from the adverse effects of climate change (e.g., high evaporation rate) and human activities (e.g., industrial and agricultural development within the catchment). The objectives of this work were to (i) evaluate the sediment characteristics due to the impact of the catchment on the lake and (ii) estimate the sedimentation rates and relate these to historical changes in sediment. Three sediment Cores collected in 2018 from Lake Qarun were sliced into 5 cm intervals, and the radionuclides ^{210}Pb and ^{137}Cs were measured using a γ spectrometer. The best validated models were the constant rate of supply (CRS) and the correct CRS(C-CRS). The results provide evidence that grain size, sediment fractions, organic matter (OM), organic carbon (OC) and sedimentation rate are all significantly influenced by agricultural and industrial activities.The geochronology models of ^{210}Pb indicated changes in the sedimentation process of Lake Qarun for 100 years that could be a vital source of information regarding changes in the regional and global hydrology. The estimated mean sedimentation rate based on the ^{210}Pb model is 0.45 ± 0.1 cm yr^{-1} that extremely close to the sedimentation rate of the ^{137}Cs marker is 0.55 cm yr^{-1} that indicates an excellent agreement in terms of sedimentation rate.

Keywords Drains · Mass accumulation rate · Grain size · ^{210}Pb and ^{137}Cs dating · Lake sediments

Introduction

Sediments have historically been utilized as environmental indicators and in tracing contamination sources and monitoring contaminants. They play an essential role in assessing contamination in natural water as they tend to accumulate and integrate over time even when the sediment levels in water are extremely low (Sansone et al. 2008). Sediment deposition in a lake occurs as soon as the lake is formed and continues throughout its life, decreasing its depths, hindering fish populations, and detrimental to recreation and to the aesthetics of natural and artificial lakes. Watersheds or drains surrounding lakes have a major influence on the input of sedimentary materials and, to some extent, their transport and deposition within lakes. Increased sediment loading in aquatic systems is one of humanity's most environmental and socioeconomic concerns (Pimentel 2006). This inflow of eroded material and other contaminants from lake catchments accelerates sedimentation and eutrophication processes (Kumar et al. 2007). Over the last 100 years, numerous lakes around the world have changes happen in sediment deposition (Xu et al. 2017). Thus, studying the impact of the discharge of drains on sediment characterization and the sedimentation rate is important in understanding the interaction between human activities and marine systems, which is critical for proper lake management and future planning.

The sedimentation patterns that act as markers of environmental changes and/or changes in the aquatic ecosystem are determined using lake chronology (Putyrskaya et al. 2015). Because of the importance of sedimentation rate to ecosystems and humans, a number of approaches have been developed and are currently being used to estimate sedimentation rates, depending on factors such data accessibility, measurement objectives, budget, and time regulations

✉ Noha Imam
nohaimam844@gmail.com; na.imam@niof.sci.eg

Salem Ghonamy Salem
salemghonamy_2007@yahoo.com

[1] Freshwater and Lakes Division, National Institute of Oceanography and Fisheries, Cairo, Egypt

[2] National Institute of Oceanography and Fisheries, 101 Kaser El Aini Street, Cairo 11516, Egypt

Published online: 24 July 2023

(Darama et al. 2019; Gonzalez Rodriguez et al. 2023). For instance, in many lakes, a combination of artificial ^{137}Cs (a half-life of 30.7 years) and natural ^{210}Pb (a half-life of 22.3 years) dating techniques has proven to be an effective tool for determining sediment/mass accumulation rates and interpreting sedimentary geochronology (Appleby 2001, 2008; Benoit and Rozan 2001; Ruiz-Fernández et al. 2009; Putyrskaya et al. 2015; Semertzidou et al. 2019). As part of the radioactive decay chain of ^{238}U, ^{222}Rn, an inert gas with a half-life of 3.825 days, decays to ^{210}Pb via a sequence of short-lived daughters. This gas run off from the rocks and soils into the surrounding fluid phase, such as air, ^{222}Rn emitted from land surfaces is responsible for the presence of ^{210}Pb in the atmosphere. The ^{210}Pb is scavenged in the atmosphere and then deposited on the Earth's surface via wet and dry precipitation. Three simple models of $^{210}Pb_{ex}$ have been developed to harmonize various human activities impact as well as geological and sediment processes (Appleby and Oldfield 1992); the constant flux-constant sedimentation (CF:CS) (Krishnaswamy et al. 1971; Appleby and Oldfield 1983), the constant initial concentration (CIC) (Appleby and Oldfield 1978; Robbins 1978) and the constant rate of supply (CRS) (McDonald and Urban 2007). Furthermore, the fallout of ^{137}Cs is widely utilized combined with ^{210}Pb for dating in sediment depending on temporal patterns of atmospheric nuclear testing.

Lake Qarun is one of Egypt's oldest lakes. It was known as Lake Moeris ("the great lake" in ancient Egyptians). Different wastes, municipal, industrial and agricultural activities, as well as pesticide contamination and a lack of sustainable wastewater treatment, have all contributed to major pollution concerns in Lake Qarun. There are significant ecological concerns of Lake Qarun. It gets fed with the suspended load of sediment that flows to the lake through the drains, which are additionally enhanced with fine sand from the border (Konsowa 2006). If the supply rates have increased due to human activities or climate change, this may have an impact on the rate of sedimentation on the lake bed that can absolutely fill the lake. For these reasons, it is necessary to investigate the impact of the drains on the lake's sedimentation rate and sediment quality in order to gain a better understanding of the sedimentation processes involved. The objectives of this study are to record the changes in sediment characteristics and sedimentation rates during the previous century, and their relations with the changes in sediment deposition history in the Lake.

Materials and methods

Description of the study area

Lake Qarun is a closed saline basin 43 m below mean sea level located between longitudes of 30° 24′ and 30° 49′ E and latitude of 29° 24′ and 29° 33′ N in the lowest part of El-Fayoum depression, about 80 km south west of Cairo (Fig. 1). Table 1 represents the geographical features of Lake Qarun, which are bounded by the desert on the northern side and agricultural fields on the south and south-eastern sides. The lake has been used as a water storage for irrigation of the El-Fayoum depression's agricultural areas, both directly from the main two drains (El-Batts and El-Wadi) and indirectly from the surrounding agricultural areas.

Sampling and sample preparation

Three core samples are collected from Lake Qarun January in 2018 during periods of the low tide using a Core sampler with 66 mm inner diameter. The cores were stored at 4° C in a refrigerator before they were opened. The Core was divided into 5 cm intervals and dried in oven at a temperature of 70° C, homogenizing and grinding prepared to radionuclides measurement. The samples were preserved in the lab and then firmly closed for 4 weeks to ensure that no radon was lost and that a state of secular equilibrium was achieved between the ^{226}Ra and their daughters.

Sediment characteristic

Folk's decantation method was used to prepare the sediment samples (1980) and sediment compositional classifications were determined according to Folk and Ward (1957).The physical properties of sediment, such as density, water content and porosity, were measured in each sliced core section. The sedimentology parameters were determined according to Folk and Ward (1957). The organic matter (OM) was measured according to Nelson and Sommers (1996) and the organic Carbon (OC) was according to Bengtsson and Enell (1986).

Radiometric measurements

The activity concentration of the natural primordial ^{238}U decay series (^{226}Ra, ^{214}Bi, ^{214}Pb and ^{210}Pb) and the artificial radionuclides ^{137}Cs have been performed using by gamma spectrometry (HpGe detector) in the samples. The HpGe detector has a relative efficiency of 50% and a resolution of 1.90 keV at 1.33 MeV line of ^{60}Co.

The detector was shielded with a 10 cm lead wall that was internally line with 2 mm copper and chilled with liquid nitrogen. Efficiency calibration was carried out by using three well-known reference materials obtained from the International Atomic Energy Agency for U, Th and K activity measurements: RGU-1, RGTh-1 and RGK-1 (IAEA 1987). The minimum spectrum acquisition accumulation time implied was 48 h. The activities of ^{226}Ra, which corresponds to the supported ^{210}Pb, were determined using its own gamma-ray

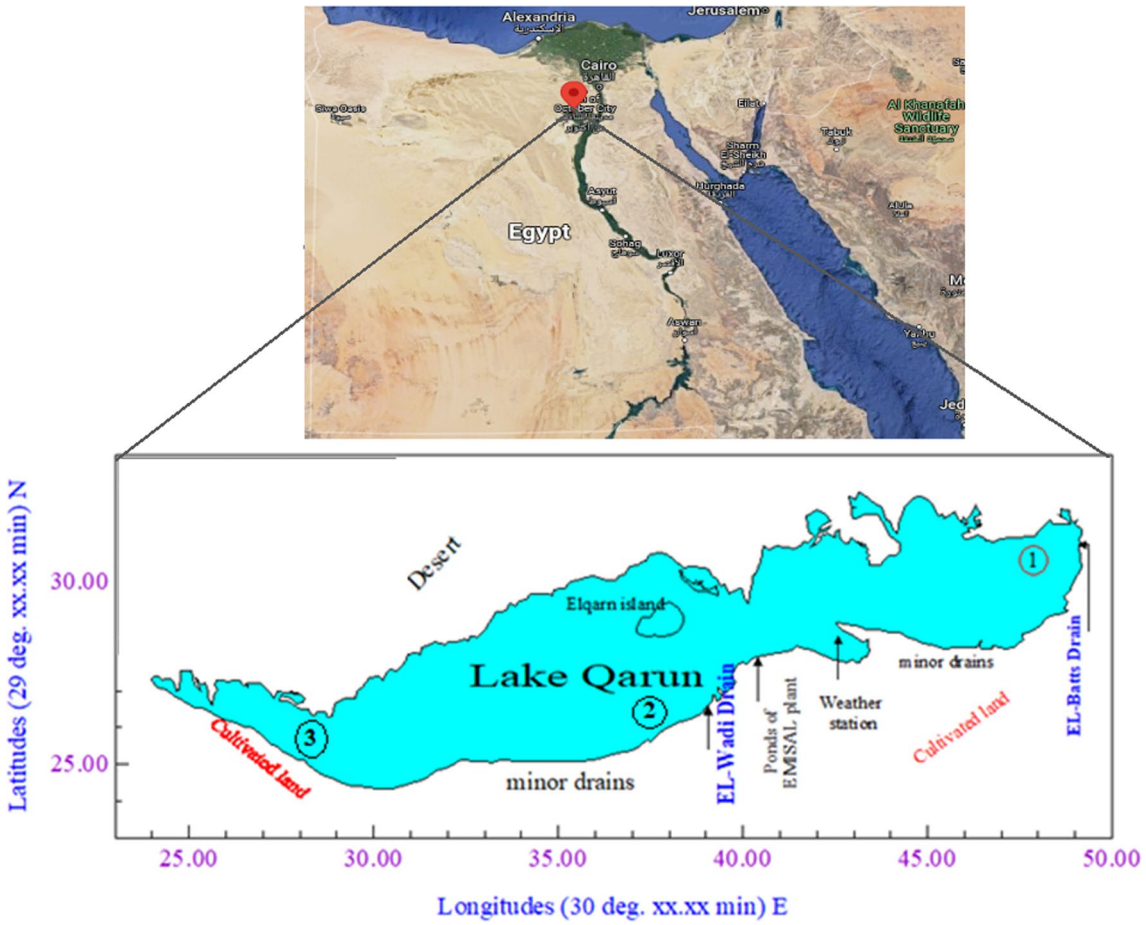

Fig. 1 Locations map of sampling sites

Table 1 Geographical features of Lake Qarun

Parameters	Lake Qarun	References
Altitude a msl (m)	43 m below	Ishak and Abdel-Malek (1980)
Latitude, Longitude	29° 24′ and 29° 33′ N and 30° 24′ and 30° 49′ E	
Surface area (km^2)	240	
Mean Depth (m)	4.2	
Length (km)	42	
Mean width (km)	5.7	
Total volume (km^3)	1	El-Shabrawy and Dumont (2009)
Water salinity (g/l)	36	
Water sources	Drainage water	
Amount of discharge	400 million m^3/year	EMISAL (1996)
Annual rainfall (mm)	9.2	Ishak and Abdel-Malek (1980)
Mean temperature (Summer) (°C)	31	
Mean temperature (Winter) (°C)	16	

186.1 keV peak after the subtraction of the 185.7 keV peak of ^{235}U and using the ^{214}Pb (295.2 and 351.9 keV peaks) and ^{214}Bi (609.3 and 1120.3 keV peaks) based on the assumption of secular equilibrium with its progenies. The activity of ^{210}Pb was measured using the 46.5 keV gamma emission. The unsupported or excess of $^{210}Pb_{ex}$ was determined by

subtracting the supported ^{210}Pb (^{226}Ra) from $^{210}Pb_{Total}$. In the same context, the activity of ^{137}Cs was determined via its gamma emission at 661.7 keV.

Theoretical aspects

Based on the radioactive decay theory, numerous geochronology models depended on the vertical profile of ^{210}Pb have been frequently utilized to date lacustrine and marine sediments (Appleby 2000; Boer et al. 2006; Sanchez-Cabeza and Ruiz-Fernandez 2012). The three major dating models depend on relative changes in $^{210}Pb_{ex}$ atmospheric deposition and sedimentation rate have been created (Sanchez-Cabeza and Ruiz-Fernandez 2012). The first model, known as the simple constant flux-constant sedimentation (CF:CS) model (Appleby and Oldfield 1992), assumes a constant flux of ^{210}Pb and constant rate of sediment deposition in the form of

$$C_i = C_0 e^{-\lambda \frac{m_i}{r}}, \tag{1}$$

where C_i is the ith layer's unsupported ^{210}Pb concentration (Bq kg^{-1}), C_0 is the water–sediment interface's $^{210}Pb_{ex}$ (Bq kg^{-1}), λ is the decay constant (0.03114 yr^{-1}).

The age t of ith layer is determined via the following the equation:

$$t = \frac{m_i}{r}, \tag{2}$$

where m_i is the cumulative mass depth to the ith layer (g cm^{-2}) and r is the mass accumulation rate (g cm^{-2} yr^{-1}).

The second model, known as the constant rate of supply model (CRS), the age t of ith layer is computed as

$$t = \frac{1}{\lambda} \ln \frac{A_0}{A_i}, \tag{3}$$

where A_0 is the total inventory of excess ^{210}Pb in the core (Bq cm^{-2}) and A_i is the total inventory of excess ^{210}Pb be low the ith layer (Bq cm^{-2}). To calcuate the mass sediment accumlation rate r_i (g cm^{-2} yr^{-1})

$$r_i = \frac{\lambda A_i}{C_i}. \tag{4}$$

The calculations using the CRS model reveal substantive discrepancies especially in the depth layers that affect on overestimation of the dating sediment. To over come this problem using C-CRS model by applying CRS model with time-bounded section, the constant $^{210}Pb_{ex}$ flux P for the section between the known dates t_1 and t_2 may be estimated as (Appleby 2000).

$$P = \frac{\lambda \Delta A}{e^{-\lambda t_1} - e^{-\lambda t_2}}, \tag{5}$$

where ΔA is the total inventory of $^{210}Pb_{ex}$ between the two reference depths x_1 and x_2 correspond to the ages $t1$ and $t2$ (t_1 sampling time) (t_2 marker of Cs-137). Age t at any depth x between x_1 and x_2 can be calculated by solving Eq. (5) as

$$t = \frac{-1}{\lambda} \ln \left(e^{-\lambda t_1} - \Delta A_{X1-X} \frac{\lambda}{P} \right), \tag{6}$$

where ΔA_{x1-x} is the total inventory of the $^{210}Pb_{ex}$ between the depths x_1 and x. The sedimentation rate r of the ith layer at time t can calcuated using the formula

$$r = \frac{P e^{-\lambda t}}{C_i}. \tag{7}$$

The third model, the constant intitial concentration (CIC) (Appleby and oldfield 1978, 1992), assumes that the initial activity of $^{210}Pb_{ex}$ remain constant irrespective of mass accumulaton rates. The activity of layer of mass depth m is:

$$C(m) = C(0) e^{-\lambda t}. \tag{8}$$

And the age of the layer (t):

$$t = \frac{1}{\lambda} \ln \frac{C_0}{C_m}. \tag{9}$$

Implications for sampling and analysis

Lake Qarun receives waste water and agricultural discharges via drains. There were precautions made during the samplings, the positions of sampling were not close to the headwaters of drains to decrease the effect of high velocities of water discharge on sediments. Quality control (QC) is performed to ensure that the analysis is accurate and to evaluate the validity and reliability of the data of ^{210}Pb using gamma spectrometry. The precision and accuracy of the analysis were estimated via the measurement of ^{210}Pb and ^{226}Ra in the certified reference materials: IAEA-RGU and IAEA-312 (soil). The measured activity concentrations were very close to the reported values of the certified materials with mean deviations and error not exceeding 3%. The precision of the gamma spectrometer system is obtained by the lowest limits of detection (LLDs), that was determined according to USDOE (1992) and Abid Imtia et al. (2005). Calcuated LLD values were 1.307, 6.5 and 0.025 Bq kg^{-1} for ^{226}Ra, ^{210}Pb and ^{137}Cs, respectively. Uncertainty of calculations of the three models is determined according to Sanchez-Cabeza and Ruiz-Fernandez (2012).

Results and discussions

Sediment characterization

The dry and wet densities of the three sediment Cores were ranged from 1.02 to 1.72 and 1.09 to 2.47 g/cm^3, respectively. The average values of the dry and wet densities were 1.4 and 2.02 g/cm^3 for Core 1, 1.61 and 2.22 g/cm^3 for Core 2, and 1.39 and 1.89 g/cm^3 for Core 3. The porosity profiles and water content of Lake Qarun showed nearly coincident behaviors with depth in Cores 1 and 3 as shown in Fig. 2a. Whereas, the porosity and water content distributions decreased with depth in the upper layers from 42 to 37% and from 36 to 29% at 15 cm, respectively.

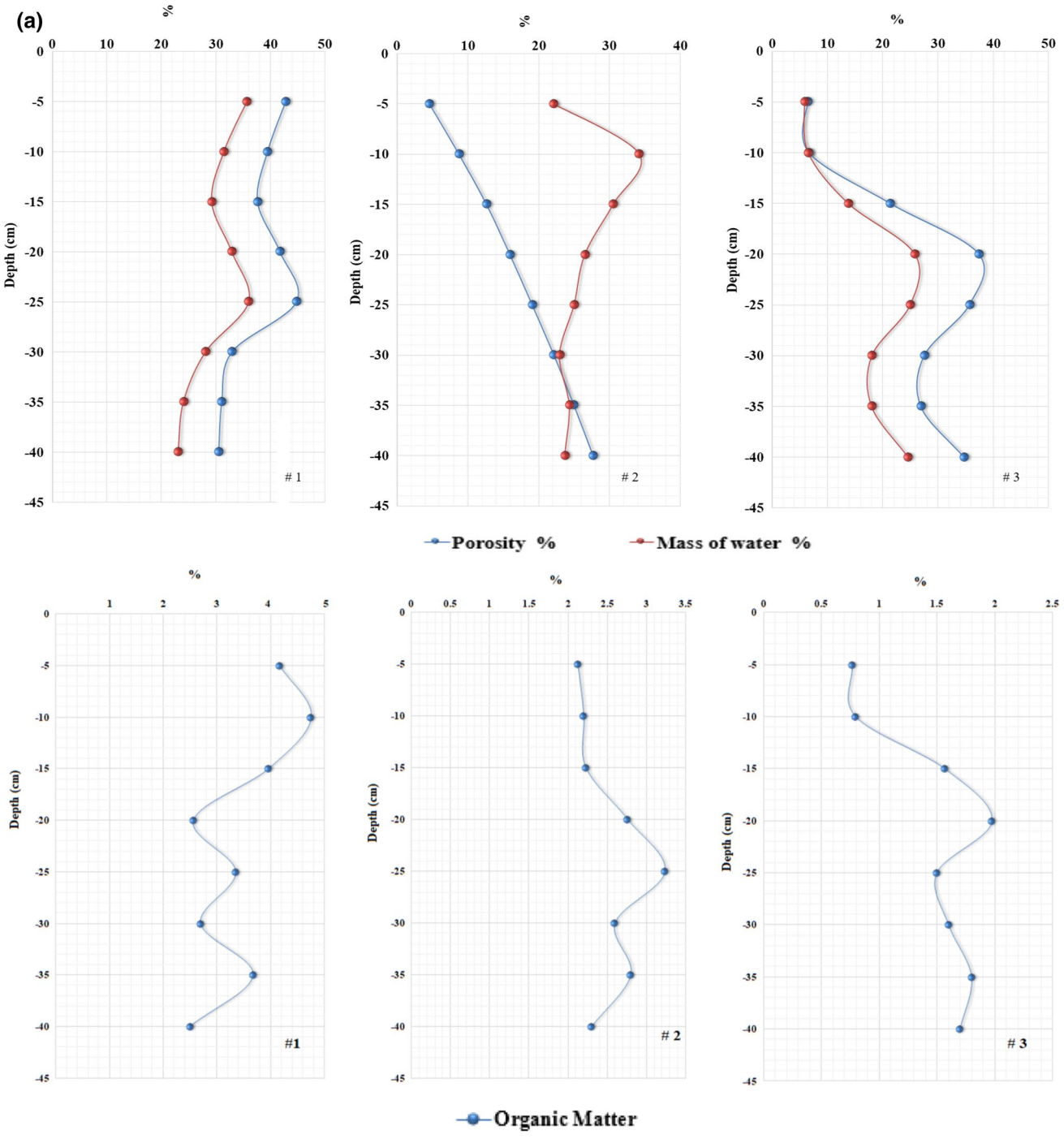

Fig. 2 **a** Porosity, the water content and the distribution of organic matter (OM); **b** vertical distributions of the grain-size fractions of core samples

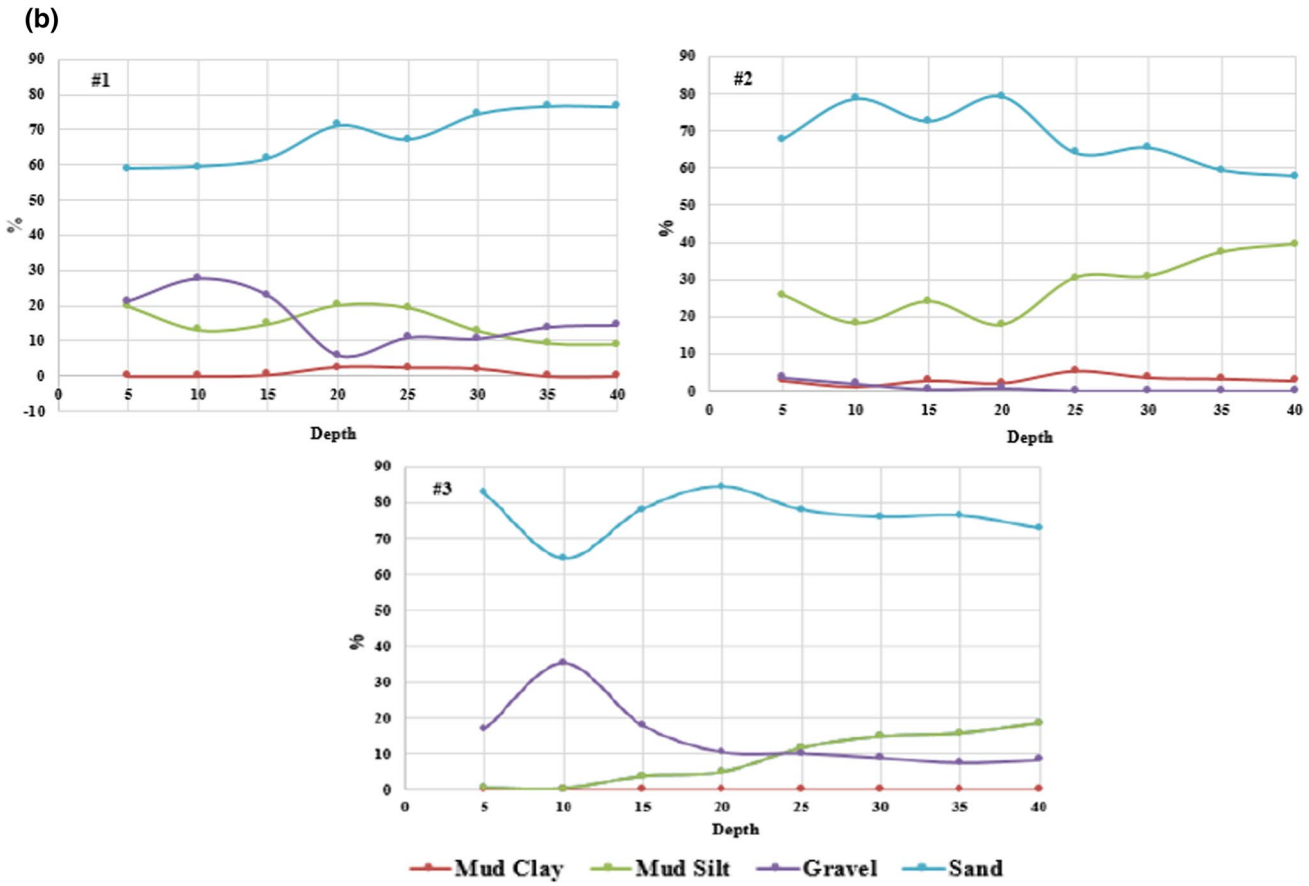

Fig. 2 (continued)

These were followed by an increase in the middle layer and a decrease again in the lower layers in Core 1. Furthermore, the porosity and water content distributions were constant in the upper layers and increased with depth and decreased in the lower layers of Core 3, which may be due to the increasing particle size with depth. Conversely, the distributions of the porosity and water content have different trends with depth and coincide in the lower layers of Core 2. The porosity profiles of the sediment Cores did not show exponential distributions. This means the sediments samples were not homogeneous with different compaction (Athy 1930). Moreover, the water content narrowly changed in Core 1 compared with those in Cores 2 and 3. This could be because of the particle size of sediments could introduce appreciable difficulty in interpreting water content trends of lake sediments.

The variations with depth of the sediment fraction textures of Lake Qarun are represented in Table 2 and Fig. 2b. Most samples could be classified as gravelly (remains of shells) muddy sand following Folk and Ward (1957) and sand fractions were predominant in the sediment Cores. The grain size distribution of Core 1 showed that gravel sediments (larger than 2 mm) varied between 5.97 and 27.51% with an average value of 15.9% and that a sand fraction (grains with diameters between 0.063 µm and 2 mm) is dominant with maximum values in the lower layers (68.3%). The mud fraction (grain size smaller than 63 µm), the second dominant fraction in the lake, ranged from 9% at 40 cm to 22.73% at 20 cm to with an average value of 15.75%. The mean grain size (Mz) was distributed as fine sand, coarse sand and very fine sand at depths of 5,10 and 25 cm, respectively, as mud at rest of Core 1. The Mz values showed a high sand content, likely representing the impact of the discharge water from the El Batts drain. Although Core 1 was not close enough to the point of discharge, the sand-rich distribution of the Core indicated that it might have been subjected to high-velocity currents where sediments were resuspended (fines washed out). Furthermore, the mean size (Mz) changed from mud in the lower layers to sand in the upper layers of the core, indicating an increase in the quantity of discharge water with time.

Sorting describes the variety of forces that influence sediment size distribution (Flok 1974; Briggs 1977) that characterize the sedimentary processes such winnowing, selective

Table 2 Fraction (%), textural classes, sedimentological parameters, percentage of organic matter (OM) and organic carbon (OC) of core samples

Core samples	Depth (cm)	Gravel (%)	Sand (%)	Mud (%)	Mud		Sediment type	Mean size (Mz)	Sorting (σ)	Skeweness (SK)	Kurtosis (K)	Organic matter (OM)%	Organic carbon (OC)%
					Silt (%)	Clay (%)							
1	0–5	21.25	58.9	19.85	19.85	0	Muddy gravelly sand	Fine sand	Very poorly sorted	Coarse skewed	Lepto urtic	4.16	2.45
	5–10	27.51	59.45	13.04	13.04	0	Muddy gravelly sand	Coarse sand	Poorly sorted	Strongly fine skewed	Very Platy Kutic	4.75	2.80
	10–15	22.7	61.8	15.5	14.8	0.37	Muddy gravelly sand	Mud	Poorly sorted	Strongly fine skewed	Lepto urtic	3.96	2.33
	15–20	5.97	71.29	22.73	20.27	2.46	Gravelly muddy sand	Mud	Poorly sorted	Fine skewed	Meso Kurtic	2.57	1.51
	20–25	11	67.23	21.77	19.5	2.27	Gravelly muddy sand	Very fine sand	Very poorly sorted	Coarse skewed	Meso Kurtic	3.35	1.97
	25–30	10.66	74.55	14.79	12.8	1.99	Gravelly muddy sand	Mud	Very poorly sorted	Near symmetrical	Lepto urtic	2.70	1.59
	30–35	13.88	76.79	9.33	9.33	0	Muddy gravelly sand	Mud	Poorly sorted	Fine skewed	Lepto urtic	3.67	2.16
	35–40	14.4	76.6	9	9	0	Muddy gravelly sand	mud	Poorly sorted	Fine skewed	Lepto urtic	2.50	1.47
2	0–5	3.7	67.67	28.63	25.85	2.78	Muddy sand	Fine sand	Very poorly sorted	Near symmetrical	Meso Kurtic	2.12	1.25
	5–10	2.02	78.77	19.21	18.14	1.07	Muddy sand	Mud	Very poorly sorted	Strongly fine skewed	Lepto urtic	2.20	1.29
	10–15	0.49	72.65	26.87	24.07	2.8	Muddy sand	Medium sand	Poorly sorted	Strongly coarse skewed	Meso Kurtic	2.23	1.31
	15–20	0.77	79.37	19.86	17.76	2.1	Muddy sand	Medium sand	Poorly sorted	Coarse skewed	Meso Kurtic	2.76	1.62
	20–25	0.05	64.08	35.87	30.41	5.45	Muddy sand	Fine Sand	Very poorly sorted	Near symmetrical	Meso Kurtic	3.24	1.91
	25–30	0.07	65.5	34.4	30.8	3.6	Muddy sand	Very fine sand	Poorly sorted	Fine skewed	Lepto Kurtic	2.60	1.53
	30–35	0.07	59.4	40.6	37.3	3.3	Muddy sand	Very fine sand	Poorly sorted	Fine skewed	Lepto Kurtic	2.80	1.65
	35–40	0.05	57.8	42.1	39.4	2.7	Muddy sand	Very fine sand	Poorly sorted	Fine skewed	Meso Kurtic	2.30	1.35

Table 2 (continued)

Core samples	Depth (cm)	Gravel (%)	Sand (%)	Mud (%)	Mud		Sediment type	Mean size (Mz)	Sorting (σ)	Skeweness (SK)	Kurtosis (K)	Organic matter (OM)%	Organic carbon (OC)%
					Silt (%)	Clay (%)							
3	0–5	16.83	82.65	0.51	0.51	0	Gravelly sand	Very fine sand	Very poorly sorted	Near symmetrical	Very Lepto Kurtic	0.77	0.45
	5–10	35.2	64.48	0.32	0.32	0	Gravelly sand	Very fine sand	Very poorly sorted	Strongly fine skewed	Very Lepto Kurtic	0.80	0.47
	10–15	18.11	78.18	3.7	3.7	0	Muddy gravelly sand	Mud	Poorly sorted	Fine skewed	Lepto urtic	1.57	0.92
	15–20	10.73	84.39	4.88	4.88	0	Muddy gravelly sand	Coarse sand	Poorly sorted	Strongly coarse skewed	Very Lepto Kurtic	1.98	1.16
	20–25	10.3	78	11.7	11.7	0	Muddy gravelly sandy	Medium sand	Poorly sorted	Near symmetrical	Very Lepto Kurtic	1.50	0.88
	25–30	9.1	76	14.9	14.9	0	Muddy gravelly sandy	Fine sand	Poorly sorted	Near symmetrical	Lepto Kurtic	1.60	0.94
	30–35	7.8	76.4	15.8	15.8	0	Muddy gravelly sandy	Fine sand	Poorly sorted	Near symmetrical	Lepto Kurtic	1.80	1.06
	35–40	8.5	72.9	18.7	18.7	0	Muddy gravelly sandy	Fine sand	Poorly sorted	Near symmetrical	Lepto Kurtic	1.70	1.00

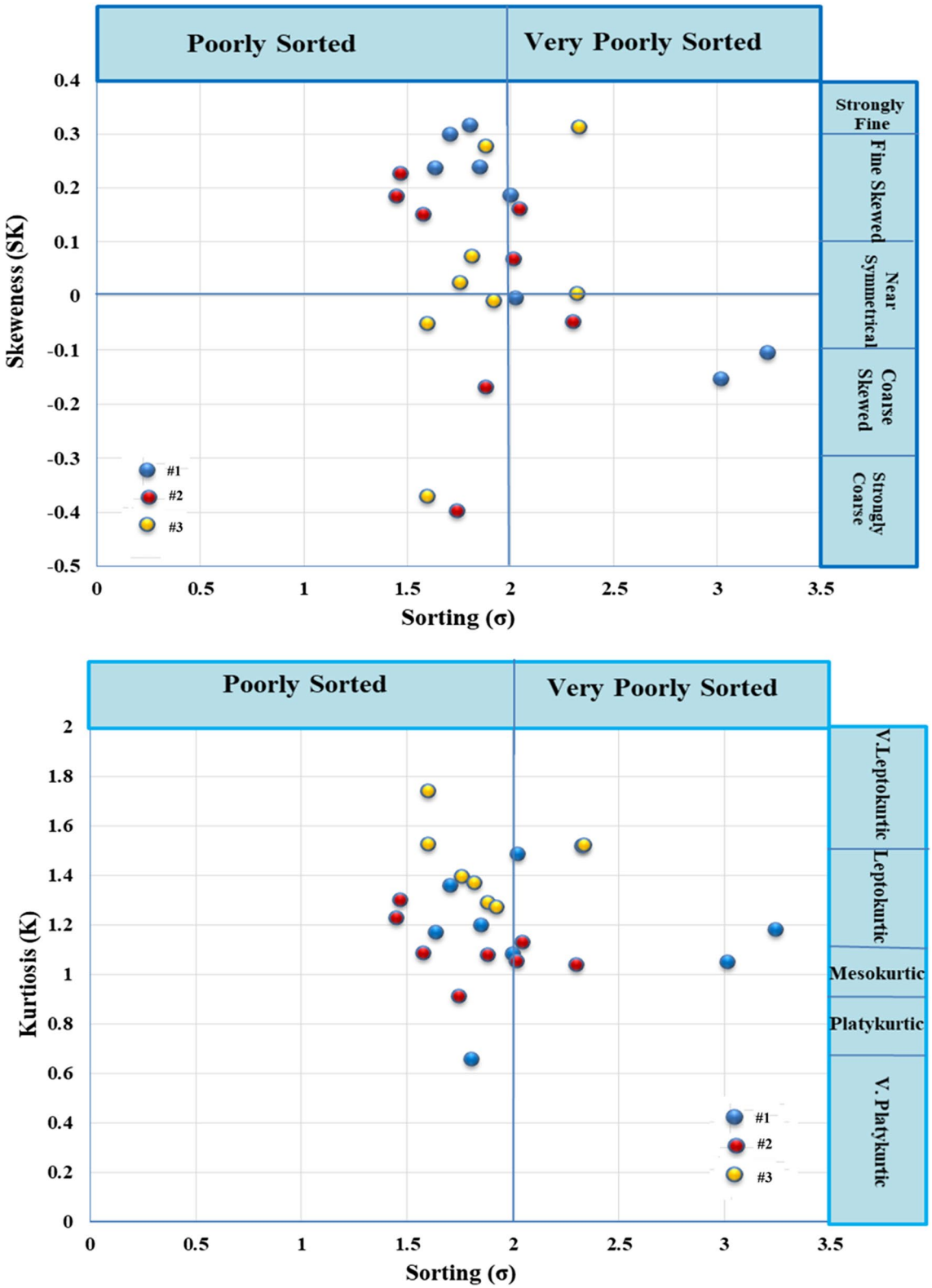

Fig. 3 Biplot of skewness vs. sorting and kurtosis vs. sorting in core samples

deposition, and total deposition as well as the direction of transport (Mclaren 1981). In Core 1, the sorting degree (σ_1) was very poorly at depths of 5, 25 and 30 cm and poorly sorted at depths 10, 15, 20,35 and 40 cm. There is a general increase in the sorting values correspond to worse sorting processes of sediment samples that varied from very poorly sorted to poorly sorted, denoting higher variability in grain size (gravel and sand gets concentrated). According to Friedman (1961), the asymmetry of a frequency distribution with respect to the median value of sediment grain size is measured by skewness. The skewness (SK_1) for Core 1 was distributed as coarse skewed at depths of 5 and 25 cm but strongly fine and fine skewed at depths of 10 and 15 cm and 20, 35 and 40 cm, respectively. According to Bhattacharya et al. (2016), the positive skewness is indicated the deposition of sediments under low energy conditions, the constant addition of finer materials, and maintaining of their original characteristics during deposition. The SK_1 was nearly symmetrical at 30 cm, indicating a uniform or regular pattern of sediment deposition (Fig. 3). These findings showed that the top 5 cm (from −0.1 to −0.3) were influenced by strong water current energy and high levels of water delivering different amounts of suspended fraction and sand fraction. While the water level and water current force were moderate at the medium layer at 30 cm (from −0.1 to 0.1), fine suspended fraction (silt and clay) was deposited at deep layers due to lower the water current force. The kurtosis (K_G) of the sediment in Core 1 was leptokurtic at depths of 5, 15, 30, 35 and 40 cm but very platykurtic at depth of 10 cm and mesokurtic at depths of (20 and 25 cm) (Fig. 3). The changes in the proportions of fine and coarse-grained particles along a Core can provide insight into how the sedimentation process has changed over time (Weaver 1994). Whereas, the El-Batts drain's velocity of water and quantity had an impact on the diversity of the sediments in the top layers of the sedimentary process. Depending on how much water was discharged, the water level and current energy changed multiple times, causing the environment for sediment deposition to change and form different layers.

Core 2 had a small gravel fraction (0.05–3.7%) and a high sand content (57.8–79.37%), and its mud fraction varied between 19.21% at a depth of 10 cm and 42.1% at a depth of 40 cm with an average value of 30.94%. The Mz of Core 2 stated fine sand at depths of 5 and 25 cm where the water current and level of the El-Wadi drain were quiet. Whereas; the water current of the El-Wadi drain being medium led into medium sand at depths of 15 and 20 cm and mud at depths of 10 cm with the water level decreasing and being very quiet, and very fine sand at depths of 30 to 40 cm. The mean grain size of Core 2 was muddy sand. The sorting degree (σ_1) fluctuated between very poorly and poorly sorted in the Core samples. The SK_1 was near symmetrical at depths of 5 and 25 cm, fine skewed at 30–40 cm, strongly fine skewed at 10 cm and strongly coarse and coarse skewed at 15 and 20 cm. The kurtosis is a measure of the mixing of two-end populations, which explains how fraction distributions take a particular form. The K_G was mesokurtic except at 10, 30 and 35 cm, where it was leptokurtic which indicating a steady deposition environment for the majority of the time.

The grain size distribution of Core 3 showed that the gravel proportion varied between 8.5 and 35.2% with an average of 14.57%. Sand fractions were the predominant in the Core, with an average value of 76.63%, whereas the mud fraction was lowest proportion with an average value of 8.81%. These findings indicated that Core 3 had less diversity in grain size than Core 1 because Core 3 was located in a desert area west of the lake, whereas Core 1 was positioned near an agricultural area to the east of the lake. The Mz was very fine sand at depths of 5 and 10 cm, mud at 15 cm, coarse sand at 20 cm, medium sand at 25 cm and fine sand at 30–40 cm. The sorting degree fluctuated between very poorly and poorly sorted as in Core 2 and 1. The degree of skewness was fickle near symmetrical at 5 and 25–40 cm, strongly fine at 10 cm, fine skewed at 15 cm and strongly coarse skewed at 20 cm. The KG was very leptokurtic except at 15 and 30–40 cm, where it was leptokurtic (Fig. 3). The sediment type in Core 3 was gravelly sand in upper layers, and the lower layers of the Core had muddy gravelly sand which may indicate changes in the velocity and quantity of water current released over the time.

Small cross-sectional areas were due to shallow depths and narrow widths, were observed in our results; higher velocities increased gravel sediments (shells and fragments) at Core 1 and 3. In contrast, in Core 2, the cross-sectional area in the discharge headwaters was greater than those in the other two Cores, causing sediments to settle upon entering the lake. Thus, the grading of predominant grain sizes from gravelly sand in high-velocity areas to mud sand in low-velocity areas is clarified. It can be seen when the average percentages of the grain size in each Core are calculated that the sand is the dominant fraction, followed by mud and then gravel. The sediment Cores of Lake Qarun are generally heterogeneous and moderately sorted ranging from coarse sand to silt that consists mainly of sand fraction and variable ratios of gravel and mud. This might be due to the different sedimentary processes. Furthermore, most of the core sediment samples were very poorly sorted, ranging from near symmetrical to strongly fine skewed, from mesokurtic to leptokurtic, as shown in Fig. 3.

The vertical distributions of the organic matter (OM) and the organic carbon (OC) are shown in Table 2 and Fig. 2a. The organic matter (OM) content of the Cores ranged from 0.77 to 4.75% with an average value of 2.48%. The maximum value is noticed in the eastern part of the lake Core 1, whereas the minimum value is observed in the western part of the lake Core 3. The percentage of OM in the near surface

Table 3 Vertical distribution of ^{210}Pb, ^{226}Ra,$^{210}Pb_{ex}$ and ^{137}Cs in core samples

Core samples	Depth (cm)	Dry mass (g)	Cumulative depth (g cm^{-2})	^{210}Pb (Bq kg^{-1})			^{137}Cs (Bq kg^{-1})
				^{210}Pb	^{226}Ra	$^{210}Pb_{ex}$	
				Total	Supported	Unsupported (excess)	
1	0–5	231	6.76 ± 0.13	30.63 ± 2.5	19.00 ± 0.57	11.62 ± 1.93	0.85 ± 0.08
	5–10	243	13.87 ± 0.27	28.23 ± 1.90	16.15 ± 0.63	12.08 ± 1.27	0.72 ± 0.07
	10–15	250	21.18 ± 0.41	26.49 ± 1.60	14.83 ± 0.55	11.66 ± 1.05	0.62 ± 0.09
	15–20	250	28.49 ± 0.55	26.82 ± 1.60	19.67 ± 0.54	7.15 ± 1.06	0.50 ± 0.07
	20–25	247	35.71 ± 0.69	27.81 ± 1.80	21.56 ± 0.49	6.25 ± 1.31	0.42 ± 0.06
	25–30	215	42 ± 0.81	31.98 ± 2.70	21.47 ± 0.49	10.52 ± 2.21	1.13 ± 0.10
	30–35	243	49.11 ± 0.95	25.55 ± 1.5	21.30 ± 0.32	4.25 ± 1.18	0.30 ± 0.04
	35–40	250	56.42 ± 1.09	22.00 ± 1.00	21.00 ± 0.31	1.00 ± 0.69	*ND
2	0–5	280	8.19 ± 0.15	27.98 ± 1.90	21.41 ± 0.32	6.58 ± 1.58	0.62 ± 0.08
	5–10	279	16.35 ± 0.30	25.22 ± 1.50	20.72 ± 0.36	4.50 ± 1.14	0.54 ± 0.07
	10–15	286	24.71 ± 0.46	28.56 ± 1.80	26.70 ± 0.73	1.86 ± 1.07	0.48 ± 0.06
	15–20	263	32.4 ± 0.60	24.74 ± 1.40	21.24 ± 0.84	3.50 ± 0.56	0.42 ± 0.05
	20–25	270	40.3 ± 0.69	27.28 ± 1.80	24.78 ± 0.60	2.50 ± 1.20	0.46 ± 0.05
	25–30	285	48.63 ± 0.85	24.50 ± 1.30	22.50 ± 0.72	2.00 ± 0.58	0.20 ± 0.01
	30–35	283	56.91 ± 1	23.70 ± 1.20	22.00 ± 0.60	1.70 ± 0.60	*ND
	35–40	290	65.39 ± 1.18	22.30 ± 1.00	22.00 ± 0.60	0.30 ± 0.40	*ND
3	0–5	189	5.53 ± 0.11	26.35 ± 1.7	11.89 ± 0.51	14.46 ± 1.19	0.34 ± 0.06
	5–10	175	10.65 ± 0.21	22.89 ± 1.4	14.66 ± 0.72	8.23 ± 0.68	0.24 ± 0.06
	10–15	291	19.16 ± 0.38	19.53 ± 1	12.38 ± 0.79	7.15 ± 0.21	0.26 ± 0.08
	15–20	294	27.76 ± 0.55	17.49 ± 1	10.53 ± 0.40	6.96 ± 0.60	0.42 ± 0.05
	20–25	285	36.09 ± 0.72	16.87 ± 0.9	11.50 ± 0.60	5.37 ± 0.30	0.20 ± 0.02
	25–30	295	44.72 ± 0.88	15.65 ± 0.85	11.00 ± 0.50	4.65 ± 0.35	0.18 ± 0.01
	30–35	287	53.11 ± 1.05	13.12 ± 0.76	10.62 ± 0.20	2.50 ± 0.56	*ND
	35–40	279	61.27 ± 1.22	12.50 ± 0.71	11.54 ± 0.30	0.96 ± 0.41	*ND

*Not detect

sediment was higher than that in the deepest part of Core 1, but it was the opposite in Cores 2 and 3. The profile of OM concentration in Core 1 decreased with depth. This is due to the recent increases in the OM deposition due to eutrophication (Emeis et al. 2000; Voss et al. 2000). There is another an essential factor contribution to this phenomenon is the mineralization of the labile portion of OM (Pempkowiak and Kulinski 2012). Moreover, the highest OM values were in Core 1 near the El-Batts drain, which acts as trap and reservoir for minerals of human activities (Camusson et al. 2002). This OM originated from biogenic production within the lake and delivery of allochthonous material. Conversely, the OM in Cores 2 and 3 had nearly similar trends that stable in upper layers and increased with depth in the middle layers and decreased in lower layers. In the same context, the organic carbon (OC) of Core 1 ranged between 2.8% at depth of 10 cm and 1.47% at a depth of 40 cm with an average value of 2.03%. Meanwhile, the highest OC value of Core 2 was at the lower layer of the Core sediment, and the lowest value was at the surface layer. Core 3 in the western part of the lake, the organic carbon (OC) fluctuated from 1.16 to 0.5% with an average value of 0.86%. The minimum value is observed in the western part of the lake, whereas the maximum is determined in the eastern part. This might be because most of the core sediments are characterized as mud (Core 1) and fine sand (Core 3). This was agreed with El-Kady et al. (2019) who recorded the sediments with abundant clay have high organic carbon content. The OC and OM profiles behaved similarly in the three Cores. The amount of organic carbon did not vary significantly along the lake's size. The Mid-Atlantic Integrated Assessment (MAIA) Estuaries ranges include high impact (> 3), intermediate impact: (1 to 3), low impact: (≤ 1%) organic carbon. The OC concentrations in the sediments of Lake Qarun were in the intermediate impact range of MAIA.

^{210}Pb and ^{137}Cs distribution

The vertical distribution of the $^{210}Pb_{total}$, ^{226}Ra and ^{137}Cs activities for the three sediment cores are represented

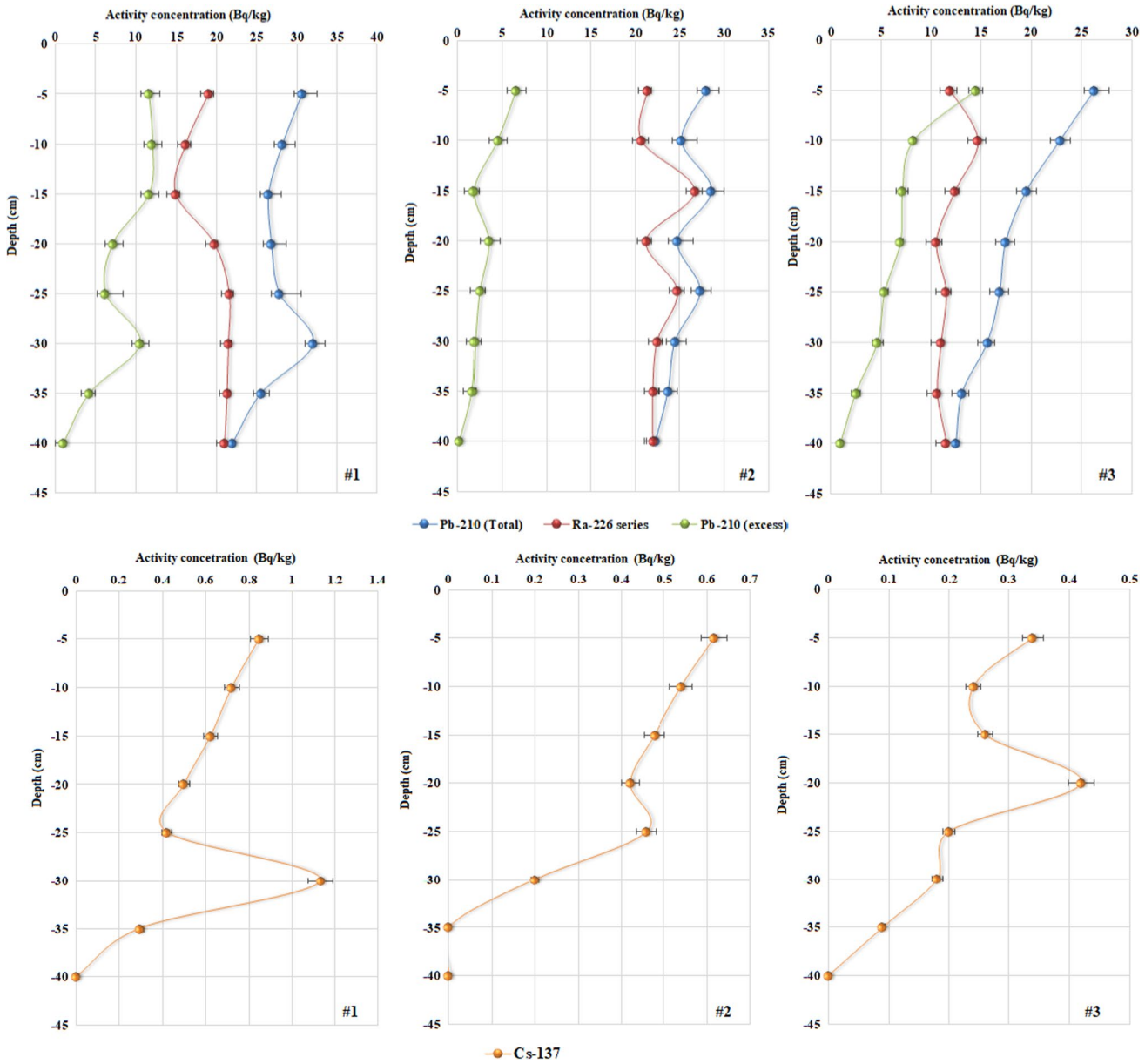

Fig. 4 $^{210}Pb_{Total}$,^{226}Ra,$^{210}Pb_{ex}$ and ^{137}Cs specific activity profiles in in core samples

Table 4 Correlation matrix of the textural components of sediment (sand, gravel and mud clay), mean grain size (Mz), organic matter (OM) and ^{137}Cs and ^{210}Pb activity concentration

Variables	Mz	Sand	Gravel	Mud	OM	Cs-137	Pb-210
Mz	1						
Sand	−0.07	1					
Gravel	0.11	0.09	1				
Mud	−0.04	−0.56	−0.81	1			
OM	0.12	−0.53	−0.01	0.41	1		
Cs-137	−0.05	−0.1	0.24	0.02	0.45	1	
Pb-210	0.04	0.05	0.72	−0.51	0.05	0.67	1

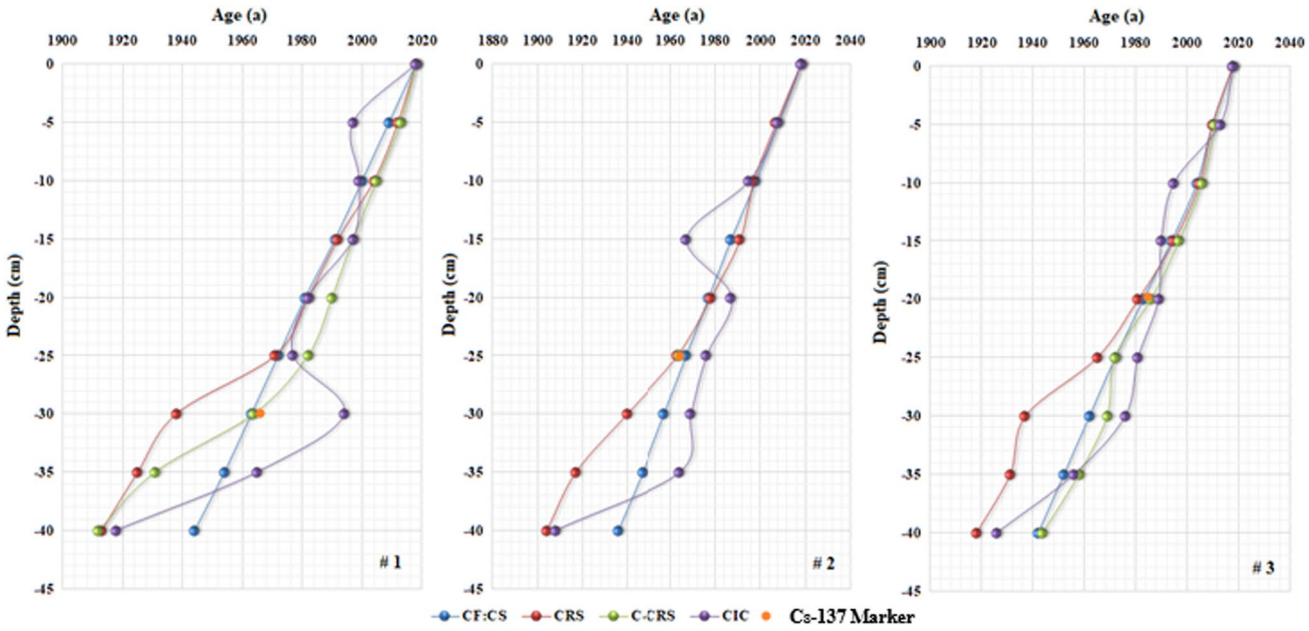

Fig. 5 Chronologies distribution derived from CF;CS, CRS,C-CRS, CIC and the Cs-137 marker in in core samples

in Table 3 and Fig. 5. The $^{210}Pb_{total}$ concentration profile showed an approximately exponential decrease with depth in Core 1 except in the lower layer and Core 3. The activity concentration of $^{210}Pb_{total}$ ranged from 22.00 ± 1.00 to 31.98 ± 2.7 Bq kg^{-1} with a maximum peak detected at 25–30 cm at Core 1 (Fig. 4). In Core 2, the activity concentration of $^{210}Pb_{total}$ had a narrow change that varied from 22.5 ± 1 to 28.56 ± 1.8 Bq kg^{-1}. Conversely, the $^{210}Pb_{total}$ activity concentration fluctuated from 12.5 ± 0.71 to 26.35 ± 1.7 Bq kg^{-1}, which decreased with depth in Core 3. The activity concentrations of ^{226}Ra, corresponding to $^{210}Pb_{supported}$ activities, varied from 10.53 ± 0.40 to 26.70 ± 0.73 Bq kg^{-1} throughout the three sediment Cores. The profile shape of ^{226}Ra could not be evaluated; hence, it was approximately constant in the lower layers of the profiles in the three Cores. The specific activity of the ^{226}Ra was irregularly distributed with narrow variations that may provide evidence of sediment mixing. The total ^{210}Pb and unsupported ^{210}Pb (excess) showed nearly exponential profiles in Cores 2 and 3. Otherwise, the activity concentration of the total ^{210}Pb and $^{210}Pb_{ex}$ in sediment Core 1 was nearly constant in the upper layers and decreased with depth in the middle layer and increased in the lower layers with the maximum concentration found in Layer 6 at 30 cm. The total ^{210}Pb activity concentration reached an equilibrium with the ^{226}Ra activity concentration at 40 cm in Core 1, at 25 cm in Core 2 and at 35 cm in Core 3.The $^{210}Pb_{ex}$ activity in the three sediment cores generally decreased exponentially with cumulative mass depth. There was a good correlation between the $^{210}Pb_{ex}$ activities and the cumulative mass depth in the three Cores (R1 = 0.63, R2 = 0.86 and R3 = 0.71)) ($n = 8$). The vertical distributions of the $^{210}Pb_{ex}$ activities, were complex and irregular, which may have been partially due to bioturbation. The activity concentrations of ^{137}Cs in the sediment cores are shown in Fig. 4. The fallout of the ^{137}Cs activity released into the atmosphere might have triggered the first globally significant levels that appeared in 1954 ± 2. The maximum peak of ^{137}Cs was detected at 25–30 cm (1.13 ± 0.10 Bq kg^{-1}) at Core 1 and at 20–25 cm (0.46 ± 0.05 Bq kg^{-1}) at Core 2, possibly corresponding to the maximum peak of the weapons fallout AD 1964. In Core 3, the maximum peak of ^{137}Cs was detected at 15–20 cm (0.42 ± 0.05 Bq kg^{-1}) which is significant may to the Chernobyl accident in 1986. The activity concentration of ^{137}Cs versus the depth profile was relatively weak in all sediment Cores. The values of the ^{137}Cs activities were most likely the effect of some factors, such as remobilization and water flow or other unusual factors in the lake. Indeed, the explanations for the mobility of ^{137}Cs probably molecular diffusion, bioturbation and resuspension (Walling and Qingping 1992). Furthermore, Sholkovitz (1983) hypothesized that the ^{137}Cs might be mobilized in saltwater environments because seawater is highly charged with monovalent cations. This is probably these cations have emigrated ^{137}Cs up the cores over the last 50 years that has caused in the remobilization and released of ^{137}Cs to the water column (Foster et al. 2006). The behavior of ^{137}Cs of in the sediments is obviously similar to that of unsupported ^{210}Pb, which may be associated with the events that produced the former in these Cores. Either ^{210}Pb or ^{137}Cs have migrated differentially by

Table 5 Comparison of the chronology and sedimentation rate in different models of the core samples

Core Samples	Depth (cm)	Pb-Cs model							
		CF:CS		CRS		C-CRS		CIC	
		Date AD	Sedimentation rate (cm yr^{-1})	Date AD	Sedimentation rate (cm yr^{-1})	Date AD	Sedimentation rate (cm yr^{-1})	Date AD	Sedimentation rate (cm yr^{-1})
1	0	2018	–	2018	–	2018	–	2018	–
	5	2009 ± 0 (0.32)	0.62 ± 0.04	2012 ± 1 (0.9)	0.73 ± 0.13	2013 ± 1 (1.3)	0.86 ± 0.26	1997 ± 6 (6.3)	0.24 ± 0.05
	10	2000 ± 1 (0.6)	0.69 ± 0.04	2004 ± 1 (0.8)	0.52 ± 0.06	2005 ± 1 (1.01)	0.64 ± 0.09	1999 ± 5 (4.8)	0.26 ± 0.04
	15	1991 ± 1 (0.9)	0.73 ± 0.04	1992 ± 1 (0.8)	0.37 ± 0.04	1997 ± 1 (1.1)	0.49 ± 0.06	1997 ± 4 (4.4)	0.24 ± 0.02
	20	1981 ± 1 (1.14)	0.68 ± 0.04	1982 ± 1 (0.9)	0.44 ± 0.07	1990 ± 1 (1.3)	0.64 ± 0.11	1982 ± 6 (5.8)	0.14 ± 0.02
	25	1972 ± 2 (1.5)	0.64 ± 0.04	1971 ± 1 (1.4)	0.36 ± 0.08	1982 ± 2 (1.9)	0.59 ± 0.13	1977 ± 8 (7.6)	0.12 ± 0.05
	30	1963 ± 2 (1.7)	0.67 ± 0.04	1938 ± 1 (1.3)	0.08 ± 0.02	1964 ± 2 (1.8)	0.23 ± 0.05	1994 ± 8 (7.6)	0.21 ± 0.02
	35	1954 ± 2 (2.1)	0.78 ± 0.05	1925 ± 2 (2.3)	0.13 ± 0.04	1931 ± 3 (3.3)	0.18 ± 0.05	1965 ± 10 (9.6)	0.09 ± 0.02
	40	1944 ± 2 (2.3)	0.81 ± 0.05	1913 ± 15 (14.8)	0.16 ± 0.13	1912 ± 21 (20.97)	0.40 ± 0.34	1918 ± 22 (22.4)	0.05 ± 0.01
2	0	2018	–	2018	–	–	–	2018	–
	5	2008 ± 0 (0.3)	1.25 ± 0.06	2007 ± 2 (1.8)	0.38 ± 0.1	–	–	2008 ± 8 (8.3)	0.48 ± 0.06
	10	1998 ± 1 (0.7)	1.19 ± 0.06	1997 ± 2 (2.01)	0.4 ± 0.1	–	–	1995 ± 8 (8.7)	0.22 ± 0.03
	15	1987 ± 1 (0.99)	1.17 ± 0.06	1991 ± 2 (2.4)	0.8 ± 0.3	–	–	1967 ± 19 (18.8)	0.1 ± 0.09
	20	1977 ± 1 (1.3)	1.03 ± 0.06	1978 ± 2 (1.7)	0.31 ± 0.05	–	–	1987 ± 6 (6.04)	0.16 ± 0.02
	25	1967 ± 2 (1.6)	1.02 ± 0.06	1963 ± 2 (2.1)	0.26 ± 0.13	–	–	1976 ± 16 (15.7)	0.12 ± 0.05
	30	1957 ± 2 (1.9)	1.04 ± 0.05	1940 ± 3 (2.8)	0.16 ± 0.04	–	–	1969 ± 10 (9.8)	0.1 ± 0.03
	35	1947 ± 2 (2.24)	0.99 ± 0.05	1917 ± 4 (3.8)	0.09 ± 0.03	–	–	1964 ± 12 (11.8)	0.09 ± 0.02
	40	1936 ± 3 (2.6)	0.98 ± 0.05	1904 ± 2 (2.1)	0.33 ± 0.3	–	–	1908 ± 43 (42.9)	0.05 ± 0.01
3	0	2018	–	2018	–	2018	–	2018	–
	5	2010 ± 0 (0.3)	0.85 ± 0.06	2010 ± 2 (1.61)	0.54 ± 0.06	2011 ± 2 (2.3)	0.6 ± 0.21	2013 ± 4 (3.6)	0.94 ± 0.03
	10	2004 ± 0 (0.4)	0.78 ± 0.06	2005 ± 2 (1.61)	0.87 ± 0.09	2006 ± 2 (2.28)	0.97 ± 0.11	1995 ± 4 (3.6)	0.21 ± 0.01
	15	1994 ± 1 (0.8)	1.10 ± 0.06	1995 ± 2 (1.61)	0.44 ± 0.02	1997 ± 2 (2.3)	0.52 ± 0.06	1990 ± 3 (2.6)	0.18 ± 0.01
	20	1983 ± 1 (1.1)	0.88 ± 0.05	1981 ± 2 (1.63)	0.30 ± 0.03	1986 ± 2 (2.28)	0.37 ± 0.04	1989 ± 4 (3.7)	0.17 ± 0.01
	25	1972 ± 1 (1.4)	0.88 ± 0.05	1965 ± 2 (1.63)	0.24 ± 0.02	1972 ± 2 (2.33)	0.27 ± 0.02	1981 ± 3 (3.04)	0.13 ± 0.01
	30	1962 ± 2 (1.8)	1.02 ± 0.05	1937 ± 2 (1.67)	0.11 ± 0.01	1969 ± 2 (2.31)	0.28 ± 0.03	1976 ± 3 (3.4)	0.12 ± 0.01
	35	1952 ± 2 (2.1)	1 ± 0.05	1931 ± 2 (2.15)	0.18 ± 0.04	1958 ± 3 (3.02)	0.37 ± 0.09	1956 ± 8 (7.6)	0.08 ± 0.01
	40	1942 ± 2 (2.4)	0.87 ± 0.05	1918 ± 6 (5.9)	0.32 ± 0.15	1944 ± 8 (8.31)	0.64 ± 0.31	1926 ± 14 (13.9)	0.05 ± 0.01

some processes other than physical mixing in this sediment (Benoit and Rozan 2001).

The conjunction of the relationship between the radionuclides ^{210}Pb and ^{137}Cs with texture components (sand, gravel and mud), mean size (Mz), organic matter (OM) and organic carbon (OC) throughout the sediment Cores was performed using a non-parametric statistical analysis (Spearman's rank correlation coefficient) summaries the findings of this study Table 4. There is a nonsignificant correlation between Mz and the activity concentration of ^{137}Cs, $^{210}Pb_{ex}$. Otherwise, there is significantly strong positive correlation between the activity concentration of ^{210}Pb and gravel sediment, while it is a weak correlation between the activity concentration of ^{137}Cs and gravel sediment. Moreover, the ^{210}Pb activity concentration is a negative correlation with mud and ^{137Cs} is nearly a nonsignificant correlation. Mud clay granules are essential in the transit and accumulation of ^{210}Pb, as evidenced by the strong relationships between clay and $^{210}Pb_{ex}$ found in previous investigations (Liu et al. 2009; Sun et al. 2017) but appeared to be difficult to assume in the lake examined. However, the organic matter (OM) and organic carbon (OC) concentrations of sediment cores showed a significant medium correlation with the activity concentration of ^{137}Cs through the study area. In the same context, an organic matter (OM) and organic carbon (OC) have an important influence on the distribution of ^{210}Pb fluxes in the sediments. The highest values of OM content and OC were in Core 1, which agrees with the highest ^{210}Pb fluxes, indicating the medium significant positive correlation between OM content, OC and ^{210}Pb fluxes in Core 1. Otherwise, there are weak negative correlation between OM content, OC and ^{210}Pb fluxes in Cores 2 and 3. The positive relationship between the ^{210}Pb fluxes and the sedimentary OM confirmed that the OM is an essential factor aiding the deposition of $^{210}Pb_{ex}$ in eutrophic lakes (Wan et al.

2005) and this is confirmed by the results of Lake Qarun in Core 1. Also, presence of radionuclides in a significant amounts in the sand fraction is highly correlated with the large levels of OM (4%). OM coatings on mineral particles have long been known to boost the adsorption capacity of dissolved radionuclides (Mejjad et al. 2016).

Chronologies and sedimentation rates

The chronologies estimated using ^{210}Pb models *constant flux: constant sedimentation* (CF:CS), *constant initial concentration* (CIC), *constant rate of supply* (CRS) and *Correct-CRS (C-CRS)* provided substantially different chronologies for the three sediment cores (Fig. 5 and Table 5).

Generally, the CRS and C-CRS models produced older ages than those of the other models (CF: CS and CIC), which gave younger ages for the lower layers of the cores. Furthermore, the CIC chronology showed multiple age inversions. This means that nonmonotonic decline with depth estimated younger dates for deeper layers for this model. The chronology obtained by the CF:CS, CRS and C-CRS models represented a good fit in the upper strata of the Cores, contrary to that in the ages estimated by the CIC model were quite different from those computed by other models. The discrepancies in the CIC model dates indicated variations in the initial ^{210}Pb concentrations due to various causes. Because the ^{210}Pb profile in this lake is nonmonotonic, the CIC model produced considerable time inversions, notably in all profiles, consistent with previous studies (Baskaran et al. 2014; von Gunten et al. 2009). The age of consecutive layers was determined using a constant flux:constant sedimentation (CF:CS) model based on the $^{210}Pb_{ex}$ appears to agree reasonably well with the ^{137}Cs-peak based chronology in the three cores as shown in Fig. 5. For the most recent sediments nearly in the top 25 cm of the three cores, there was a good agreement between the age estimates from the CF:CS and the CRS models. The age estimates from the CF:CS model were consistently younger than those from the CRS model below that depth. The unbounded CRS model failed to produce the proper age for the ^{137}Cs bomb peak (AD 1964 ± 1) in Core 1 and the Chernobyl accident (AD 1986 ± 1) in Core 3, and had to be constrained using the correct CRS (C-CRS) model. Nevertheless, the unbounded CRS model in Core 2 successfully produces the ^{137}Cs bomb peak at AD 1964 ± 1 that is highly consistent. It's clear that the CF:CS model based on $^{210}Pb_{ex}$ age was consistent with the ^{137}Cs time-marker but it gave ages younger than the true values especially in the lower parts of the cores.

In using the CRS model, the input of surplus ^{210}Pb to the sediment at a specific location is assumed to be relatively uniform over some time at least close enough to the age of the core. The total inventory of $^{210}Pb_{ex}$ is required for estimating the chronology using the CRS model, which indicated extensive range in the three cores. The total inventories of $^{210}Pb_{ex}$ were 0.447 ± 0.02 Bq cm^{-2}, 0.186 ± 0.01 Bq cm^{-2} and 0.356 ± 0.02 Bq cm^{-2} in Cores 1, 2 and 3, respectively. The total $^{210}Pb_{ex}$ inventory in Core 1 is higher than those of Cores 2 and 3, respectively. The mean annual flux of $^{210}Pb_{ex}$ was 139.2 ± 6.23 Bq m^{-2} yr^{-1}, 57.92 ± 3.12 Bq m^{-2} yr^{-1} and 110.86 ± 6.23 Bq m^{-2} yr^{-1} in cores 1, 2 and 3, respectively. Assuming uniform flux within a layer, the mean value of ^{210}Pb flux is 102.7 ± 5.2 Bq m^{-2} yr^{-1} for the three sediment Cores. The atmospheric flux of $^{210}Pb_{ex}$ can vary with the latitude depending on multiple factors, such as rainfall regime (Appleby 1998) and geographical location (Liu et al. 2012). The regional conditions of Lake Qarun located in dry zones with arid weather and low rainfall would explain low ^{210}Pb flux values. The mean values of the ^{210}Pb fluxes of Lake Qarun were obviously higher than the mean annual ^{210}Pb atmospheric flux in Lakes Edku, Burullus and Manzala (12–25 Bq m^{-2} yr^{-1}) (Appleby et al. 2001) and lakes in Chile and Bolivia, South America (Cisternas et al. 2001). The estimated $^{210}Pb_{ex}$ flux is similarly compatible with the mean ^{210}Pb atmospheric flux of 160 Bq m^{-2} yr^{-1} over continents in the latitudinal ranges of 10–30 N.

Both CRS and C-CRS models were applied, the calculations for each stratigraphic level are depicted in Fig. 5. The chronology of the CRS model was much closer and more consistent with the ^{137}Cs peak marker in Cores 2. Otherwise in the lower part of the profile Core 1, the CRS model showed approximately 26 years older ages compared with C-CRs model. Furthermore, the CRS model was older than the ages obtained with C-CRS model with 5–7 years in the middle part of the profile Core 3. We assign the ^{137}Cs atmospheric fallout peak at 30 cm as 1964 reference time marker to correct the CRS ages of $^{210}Pb_{ex}$, and then t_1 is sampling year and t_2 is 1964 in core 1 as provided in Fig. 5 and Table 5. Also, the ^{137}Cs peak of the Chernobyl accident was assigned at 20 cm as the1986 reference time marker to correct the chronology of CRS model in Core 3. It has been shown that the CRS chronologies at the bottom of ^{210}Pb profiles are overestimated and this finding observed before (e.g., McCall et al. 1984; Turner and Delorme 1996; Carroll and Lerche 2003). This conclusion is especially important for climate reconstructions since early-period calibration or cross-validation would compromise the calibration or verification statistics, resulting in very substantial forecast errors for down-core reconstructions (Cook et al. 1994). Although small tracers of ^{137}Cs were found in all sediment Cores, indicating the commencement of weapons fallout, this is interesting to validate using the CRS model. This effect could be attributed to the physical and biological mixing of newly collected sediment, and the diffusion of mobile organisms in interstitial pore water. A clear ^{137}Cs peak appeared in the 25–30 cm depth interval of Cores 1 and 2 (Fig. 4), and was assigned a date of 1964 ± 2 (i.e. maximum peak

of atmospheric fallout). Similarly, there was record of significant peak of the ^{137}Cs marker of the Chernobyl accident (AD 1986 ± 1) in the Core 3. This indicated that the 1986 Chernobyl chronomarker is available in our examined lake.

The CF:CS, CRS and C-CRS models gave internally consistent results between AD 2018 and AD 1970 but diverged significantly between 10 and 30 years in the 1st half of the nineteenth century. The results illustrated that the validation models were the CF:CS, CRS and C-CRS, whereas the most rejected model was the CIC. The watersheds' erosional input could contribute significantly to the ^{210}Pb inventory which is evidenced by differences in the initial ^{210}Pb concentrations and sedimentation rates. This indicated the failure of assuming a constant sedimentation rate and CIC of ^{210}Pb (Abril and Brunskill 2014). Thus, the C-CRS model may be more appropriate for Lake Qarun which is a closed lake mainly fed by agricultural drainage water and precipitation; also the sedimentation rate may not have been uniform due to disturbed of water discharge.

The sedimentation rates and mass accumulation rate estimated using the CRS and C-CRS models are illustrated in Table 5 and Fig. 6. The CRS model assumptions are as follows: the mass sediment accumulation rate and sedimentation rates were estimated across the sediment profile and all values determined using Eq. (4) are shown in Fig. 6. The sedimentation rates ranged from 0.08 ± 0.02 cm yr^{-1} (0.11 ± 0.03 g cm^{-2} yr^{-1}) at 30 cm to 0.73 ± 0.13 cm yr^{-1} (0.99 ± 0.18 g cm^{-2} yr^{-1}) at 5 cm with an average value of 0.35 ± 0.08 cm yr^{-1} (0.49 ± 0.1 g cm^{-2} yr^{-1}) in Core 1. No regular changes in the sedimentation rates based on sediment core depth were observed, as they may increase or decrease at any time. However, these values accelerated over time after 1940s to 1980, somewhat decreased during 1980s to1990s and rapidly increased after the 1990s to 2010s (Fig. 6). The sedimentation rates increased through time probably because of huge water discharge into the lake via drains. Similarly, in the calculation of the sedimentation rates in Core 2, it fluctuated between 0.09 ± 0.01 cm yr^{-1} (0.15 ± 0.02 g cm^{-2} yr^{-1}) to 0.8 ± 0.1 cm yr^{-1} (1.34 ± 0.16 g cm^{-2} yr^{-1}) with an average value of 0.34 ± 0.07 cm yr^{-1} (0.56 ± 0.1 g cm^{-2} yr^{-1}). Apparently, there is successive increasing in the sedimentation rate from 1920s to 1980 and there is a high increase recorded at the beginning of the 1990s and sharp decreases in the end of 1990s and near stability during 2000s in Core 2. Consequently, these appeared inconsistent with the sedimentation rates observed in Core 1. Conversely, the sedimentation rates varied from 0.11 ± 0.01 cm yr^{-1} (0.19 ± 0.01 g cm^{-2} yr^{-1}) to 0.87 ± 0.09 cm yr^{-1} (0.89 ± 0.12 g cm^{-2} yr^{-1}) with an average value of 0.38 ± 0.06 cm yr^{-1} (0.52 ± 0.08 g cm^{-2} yr^{-1}) in Core 3. There was a significant difference between the mass sediment accumulation rates and sedimentation rates obtained in Core 3 due to the change in bulk density between the profile layers (Fig. 6). Additionally, there was sequential increasing in the sedimentation rate from 1940s to the middle of 2000s and then decreasing to 2010s. Likewise, using the $^{210}Pb_{ex}$ dating model of C-CRS, the sedimentation rates and mass accumulation rates were calculated for each sample. The lowest sedimentation rate was 0.18 ± 0.05 cm yr^{-1} (0.25 ± 0.07 g cm^{-2} yr^{-1}) recording during 1930s and the highest value was 0.86 ± 0.26 cm yr^{-1} (1.17 ± 0.36 g cm^{-2} yr^{-1}) recording during 2010s in Core 1. Otherwise, the highest value of sedimentation rate in Core 3 was 0.97 ± 0.11 cm yr^{-1} (0.99 ± 0.15 g cm^{-2} yr^{-1}) recording during 2000s and the lowest value was 0.27 ± 0.02 cm yr^{-1} (0.45 ± 0.03 g cm^{-2} yr^{-1}) recording during 1970s. According to the chronology of the C-CRS was well constrained by the ^{137}Cs reference date, the average sedimentation rate was 0.50 ± 0.1 cm yr^{-1}, 0.34 ± 0.07 cm yr^{-1} and 0.50 ± 0.1 cm yr^{-1} for Cores 1, 2 and 3, respectively. However, the sedimentation rate calculated using the ^{137}Cs age marker is 0.56 cm yr^{-1}, 0.46 cm yr^{-1} and 0.63 cm yr^{-1} for Cores 1, 2 and 3 which was very close to the mean sedimentation rates in Lake Qarun estimated using the C-CRS model. Interestingly, all the mean values of the sedimentation rates estimated by the C-CRS model in Cores 1, 2 and 3 in Lake Qarun (Table 5) were nearly agree with the average value found by Flower et al. (2006).

The implications of drains on recent sediment

The size of sediment grains is modelled past lake inflow stream strength (Sundborg and Calles 2001). The grain sizes of the sediments deposited on the lake floor were controlled by the nature of the sediment source and the energy level of the sediment-transporting processes (Graham and Rea 1980), which are frequently utilized in reconstructing environmental histories (Liu et al. 2016; Macumber et al. 2018). The historical changes in the grain-size distributions of the sediment cores due to drainage water discharge into the lake were indicated through the relationship between the mean grain-size in the cores and the calendar date. In Core 1, from the1910s to the1960s, the most dominant sediment type was evidently silt mud relatively stable around 5 Ø, followed by decreased during half of the 1960s to 1980s dominated by unconsolidated very fine sands, then returned to silt mud during the 1990s, converted sharp into coarse sand during the 2000s and turned into fine sand after 10 years (2010s). Before 1960s, when human disturbance was low, lake sediments around Core 1 revealed a practically constant state in sedimentation rate (e.g. less than 0.2 cm yr^{-1}), OM and OC with slit mud grained particles. Due to large-scale agricultural and industrial activity between the 1960s and 1980s, Lake Qarun saw changes in water flow rates, which modified the grain size of sediment supply, causing an increase in sedimentation rate and a drop in OM and OC. Variations

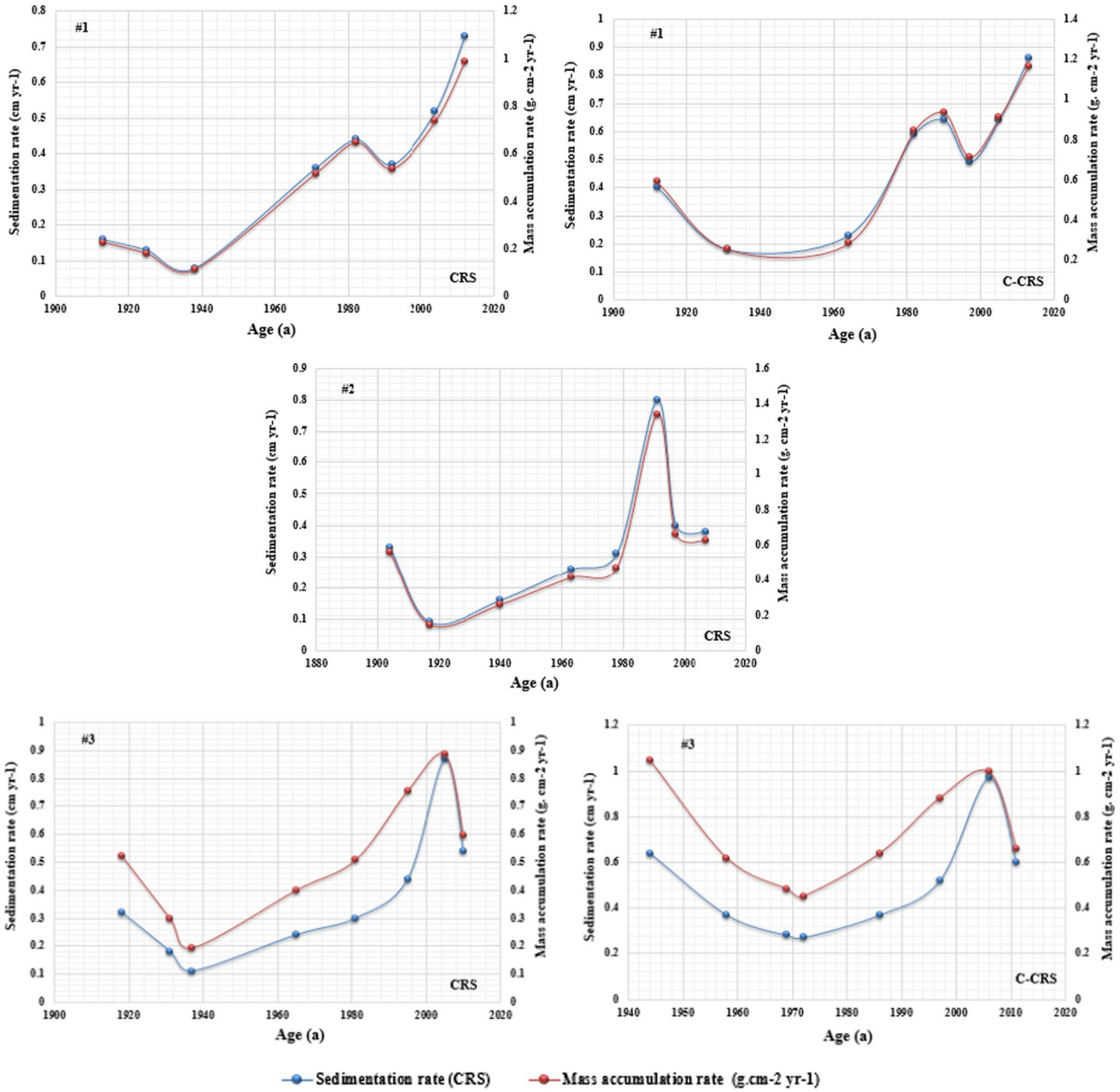

Fig. 6 Variations of sedimentation rate, mass accumulation rate with age estimated for core samples

in sedimentary environments were mirrored in the 1990s by slit mud particle size, which increased in OM and OC while decreasing in sedimentation rate, indicating changes in transport and depositional processes. Following the 1990s, coarse-grained sediments deposited closest to Core 1 showed a drop in OM and OC with increased in sedimentation rate. The results showed that grain size is a good proxy for stream discharge and that it agrees with the data (e.g., Sundborg and Calles 2001; Gilbert and Butler 2004; Van Hengstum et al. 2007). Similarly, in Core 2, from the 1920s to beginning of the 1980, the dominant sediment texture was very fine and fine sand, which relatively stable in the sedimentation rates, OM and OC, turned into medium sand with sharp increase in the sedimentation rate during the 1980s, at beginning of 1990s changed into silt mud with decreased in the sedimentation rate and returned to fine sand during the 2000s. In Core 3, the sediment texture was medium sand during the 1940s to 1980s with stability in OM and OC, and the type of grain size if sediment changed to silt mud at halfway through the 1990s and into very fine sand during the 2000s to 2010.

Overall, the historical records of sediment particle size, OM, OC concentrations, and sedimentation rate provide

insight into how anthropogenic disturbances impact sediment transport. Since the 1960s, increasing agricultural and industrial expansion has exposed Lake Qarun to high levels of anthropogenic contaminants from agriculture, as well as domestic and industrial wastes. The changes in sedimentation rates (acceleration or reduction) reflect the impact of different factors such as erosion, mixing and variation in precipitations because a deposit is a combination of numerous processes, sediment transport and deposition processes are typically challenging to represent as a simple particle size index (Beierle et al. 2002). Perhaps, the geographical distribution and anthropogenic can impact sedimentology processes of Lake Qarun. Prior to the 1960s, when there were few human activities, the sediments within discharge areas were generally very variable (ranging from sand to slit mud) as a result of the low rate of water discharge. Since 1990s, this study indicated decrease in sedimentation rates with an increase in the proportion silt mud which may be due to some developments solution to these environmental problems of Lake Qarun to achieve sustainable development of the lake during this period. In 2000s with the development of the drainage system, there is an increase in the agricultural activities that caused a huge water discharge with suspended sediment into Lake Qarun which could also influence the grain size of sediment supply. A historical perspective will provide insight into how sediment transport and the accompanying drainage change altered in the past, which will be useful in guiding future erosion control efforts. The partitioning of the grain-size components of sediments deposited in lakes could provide important information regarding historical changes in regional hydrology and global atmospheric circulation.

Conclusions

Natural environmental changes, together with human activities, significantly threaten the ecosystems of Lake Qarun, resulting in unfavorable lake environments with increased sedimentation, lower storage capacity, and changed in sediment characterizations. Understanding the pattern of drains and their impact on the sedimentation process in the lake is necessary to provide important information for sustainable lake management. This study highlights how drainage water with sediment load discharged into Lake Qarun have historically been impacted the sediment characteristics and sedimentation rates in the lake. Due to varied the sedimentary processes, the sediment Cores of Lake Qarun are generally heterogeneous and somewhat sorted, ranging from coarse sand to silt mud. The amount of organic matter and organic carbon did not differ considerably along the lake's shoreline, indicating that clay sediment contains more organic matter and organic carbon than sand particles. Bottom lake sediments are essential archives of the lake's history as well as human indications of its catchment. Our results represented that the historical records of sediment may help guide future erosion control efforts by providing information into how sediment movement and the associated drainage alteration changed in the past. As a result, appropriate lake management with sustainable land use in the lake's watershed, such as the developing eco-agricultural modes and reasonable city planning, may help prevent the lake's deterioration. One of the proposed Lake Qarun management strategies is maintaining the lake's reference conditions, which are defined by the European Union as the state of the environment prior to massive human modifications, which can be achieved by lake managers and local governments.

Authors contributions Conceptualization, validation, material preparation, data analysis, writing—original draft, review and editing were performed by NI. Validation, sampling and investigation were performed by SG. All authors read and approved the final manuscript.

Funding This research was supported by National Institute of Oceanography and Fisheries.

Availability of data and materials The datasets and materials used during the current study are available from the corresponding author on reasonable request.

Declarations

Competing interests The authors declare no competing interests.

Ethics approval and consent to participate Not applicable.

Consent for publication Not applicable.

Conflict of interest The authors declare no competing interests.

References

Abid Imtia M, Begum A, Mollah AS, Zaman MA (2005) Measurements of radioactivity in books and calculations of resultant eye doses to readers. Health Phys 88:169–174

Abril JM (2003) Difficulties in interpreting fast mixing in the radiometric dating of sediments using ^{210}Pb and ^{137}Cs. J Paleolimnol 30:407–414

Abril JM (2004) Constraints on the use of ^{137}Cs as a time-marker to support CRS and SIT chronologies. Environ Pollut 129:31–37

Abril JM, Brunskill GJ (2014) Evidence that excess ^{210}Pb flux varies with sediment accumulation rate and implications for dating recent sediments. J Paleolimnol 52:121–137

Appleby PG (2000) Radiometric dating of sediment records in European mountain lakes. Limnology 59(s1):1–14. https://doi.org/10.4081/jlimnol.2000.s1.1

Appleby PG (2001) Chronostratigraphic techniques in recent sediments. In: Last WM, Smol JP (eds) Tracking environmental change using lake sediments, volume 1: basin analysis, coring, and chronological techniques. Kluwer Academic Publishers, Dordrecht, pp 171–203

Appleby PG (2008) Three decades of dating recent sediments by fallout radionuclides: a review. Holocene 18(1):83–93
Appleby PG, Oldfield F (1978) The calculation of lead-210 dates assuming a constant rate supply of unsupported ^{210}Pb to the sediment. CATENA 5:1–8
Appleby PG, Oldfield F (1983) The assessment of ^{210}Pb from sites with varying sedimentation accumulations rates. Hydrobiology 103:29–35
Appleby PG, Oldfield F (1992) Application of lead-210 to sedimentation studies. In: Ivanovich M, Harman RS (eds) Uranium-series disequilibrium: application to earth, marine and environment sciences. Clarendon Press, Oxford, pp 731–738
Appleby PG (1998) Dating recent sediments by ^{210}Pb: problems and solutions. In: Proceedings of a seminar, STUK, Helsinki, vol 2, pp 7–24
Athy LF (1930) Density, porosity and compaction of sedimentary rocks. Bull Am Assoc Pet Geol 14:1–24
Baskaran M, Nix J, Kuyper C, Karunakara N (2014) Problems with the dating of sediment core using excess 210Pb in a freshwater system impacted by large scale watershed changes. J Environ Radioact 138:355–363. https://doi.org/10.1016/j.jenvrad.2014.07.006
Beierle BD, Lamoureux SF, Cockburn JMH, Spooner I (2002) A new method for visualizing sediment particle size distributions. J Paleolimnol 27(2):279–283. https://doi.org/10.1023/A:1014209120642
Bengtsson L, Enell M (1986) Chemical analysis. In: Berglund BE (ed) Handbook of holocene palaeoecology and palaeohydrology. Wiley, Chichester, pp 423–445
Benoit G, Rozan TF (2001) ^{210}Pb and ^{137}Cs dating methods in lakes: a retrospective study. J Paleolimnol 25:455–465
Bhattacharya RK, Das Chatterjee N, Dolui G (2016) Grain size characterization of instream sand deposition in controlled environment in river Kangsabati, West Bengal. Model Earth Syst Environ 2(3):1–14. https://doi.org/10.1007/s40808-016-0173-z
Boer W, van den Bergh GD, de Haas H, de Stigter HC, Gieles R, van Weering TJCE (2006) Validation of accumulation rates in Teluk Banten (Indonesia) from commonly applied ^{210}Pb models, using the 1883 Krakatau tephra as time marker. Mar Geol 227(3–4):263–277. https://doi.org/10.1016/j.margeo.2005.12.002
Briggs D (1977) Sources and methods in geography: sediments. Butterworths, London, p 192
Camusso M, Galassi S, Vignati D (2002) Assessment of river Po sediment quality by micropollutant analysis. Water Res 36:2491–2504
Carroll J, Lerche I (2003) Sedimentary processes: quantification using radionuclides. Elsevier, Oxford
Cisternas M, Araneda A, Martínez P, Pérez S (2001) Effects of historical land use on sediment yield from a lacustrine watershed in central Chile. Earth Surf Process Landf 26:63–76
Cook ER, Briffa KR, Jones PD (1994) Spatial regression methods in dendroclimatology—a review and comparison of 2 techniques. Int J Climatol 14:379–402. https://doi.org/10.1002/joc.3370140404
Darama Y, Selek Z, Selek B, Mehmet Ali A, Dagdeviren M (2019) Determination of sediment deposition of Hasanlar Dam using bathymetric and remote sensing studies. Nat Hazards 97(1):211–227. https://doi.org/10.1007/s11069-019-03635-y
El-Kady AA, Wade TL, Sweet ST et al (2019) Spatial distribution and ecological risk assessment of trace metals in surface sediments of Lake Qaroun. Egypt Environ Monitor Assess 191:413. https://doi.org/10.1007/s10661-019-7548-3
El-Shabrawy GM, Dumont HJ (2009) The Fayum depression and its lakes. In: Dumont HJ (ed) The Nile origin, environments, limnology and human use, vol 89. Springer, Dordrecht, pp 95–124
Emeis KC, Struck U, Leipe T, Pollehne F, Kunzendorf H, Christiansen C (2000) Changes in the C, N, P burial rates in some Baltic Sea sediments over the last 150 years—relevance to P regeneration rates and the phosphorus cycle. Mar Geol 167(1–2):43–59
EMISAL (Egyptian Company of Salts and Minerals) (1996) Qarun Lake, a base for an advanced chemical industry complex, investment opportunities based on salt extraction from Lake Qarun and the integrated industries based on it. Egyptian Salts and Minerals Co. Ltd, London
Flower RJ, Stickley C, Rose NL, Peglar S et al (2006) Environmental changes at the desert margin: an assessment of recent paleolimnological records in Lake Qarun, Middle Egypt. J Paleolimnol 35(1):1–24
Folk RL (1974) Petrology of sedimentary rocks. Hemphill, Austin, Texas, pp l–57
Folk RL (1980) Petrology of sedimentary rocks. Hemphills Publ Co, Austin, p 170
Folk RL, Ward WC (1957) Brazos River bar, a study in significance of grain size parameters. J Sediment Petrol 27:3–27
Foster IDL, Mighall TM, Proffitt H, Walling DE, Owens PN (2006) Post-depositional 137Cs mobility in the sediments of three shallow coastal lagoons, SW England. J Paleolimnol 35:881–895
Friedman GM (1961) Distribution between dune beach and river sands from their textural characteristics. J Sedimentary Petrol 31:514
Gilbert R, Lamoureux S (2004) Processes affecting deposition of sediment in a small, morphologically complex lake. J Paleolimnol 31(1):37–48. https://doi.org/10.1023/B:JOPL.0000013279.78388.24
Gonzalez Rodriguez L, McCallum A, Kent D, Rathnayaka C, Fairweather H (2023) A review of sedimentation rates in freshwater reservoirs: recent changes and causative factors. Aquat Sci 85(2):1–19. https://doi.org/10.1007/s00027-023-00960-0
Graham EJ, Rea DK (1980) HURON. J Great Lakes Res 6(2):129–140. https://doi.org/10.1016/S0380-1330(80)72091-9
Hooke RLB (1994) On the efficacy of humans as geomorphic agents. GSA Today 4:217 (**224–225**)
International Atomic Energy Agency, IAEA (1987) Preparation and certification of IAEA gamma spectrometry reference materials, RGU-1, RGTh-1 and RGK-1. International Atomic Energy Agency. Report-IAEA/RL/148
IAEA (2004) Sediment distribution coefficients and concentration factors for biota in the marine environment. IAEA Report 422. Vienna
Ishak MM, Abdel-Malek SA (1980) Some ecological aspects of Lake Qarun, Fayoum, Egypt. Part I. Physico-chemical environment. Hydrobiologia 74:173–178. https://doi.org/10.1007/BF00014569
Jweda J, Baskaran M (2011) Interconnected riverine lacustrine systems as sedimentary repositories: a case study in southeast Michigan using excess ^{210}Pb- and ^{137}Cs based sediment accumulation and mixing models. J Great Lakes Res 37:432–446
Konsowa AH (2006) Food habits of most common fishes inhabiting Lake Qarun (El-Fayoum, Egypt). J Exp Biol (Zool) 2:47–53
Krishnaswamy S, Lal D, Martin JM, Meybeck M (1971) Geochronology of lake sediments. Earth Planet Sci Lett 11(1–5):407–414
Kumar B, Rai SP, Nachiappan RP, Saravana Kumar U, Singh S, Diwedi VK (2007) Sedimentation rate in North Indian lakes estimated using ^{137}Cs and ^{210}Pb dating techniques. Curr Sci 92(10):1416–1420
Liu S, Shi X, Liu Y (2009) Sedimentation rate of mud area in the East China Sea inner continental shelf. Marine Geol Quarter Geol (in Chinese) 29(6):1–6
Liu SW, Narentuya Xia BR, Chu GQ, Tian MZ (2012) Using Pb-210(uns) and Cs-137 to date recent sediment cores from the Badain Jaran Desert, Inner Mongolia, China. Quat Geochronol 12:30–39
Liu X, Vandenberghe J, An Z, Li Y, Jin Z, Dong J, Sun Y (2016) Grain size of Lake Qinghai sediments: Implications for riverine input and Holocene monsoon variability. Palaeogeogr Palaeoclimatol Palaeoecol 449:41–51

Macumber AL, Patterson RT, Galloway JM et al (2018) Reconstruction of Holocene hydroclimatic variability in subarctic treeline lakes using lake sediment grain-size end-members. Holocene 28(6):845–857

McCall PL, Robbins JA, Matisoff G (1984) Cs-137 and Pb-210 transport and geochronologies in urbanized reservoirs with rapidly increasing sedimentation-rates. Chem Geol 44:33–65. https://doi.org/10.1016/0009-2541(84)90066-4

McDonald CP, Urban NR (2007) Sediment radioisotope dating across a stratigraphic discontinuity in a mining-impacted lake. J Environ Radioact 92:80–95

Mclaren PL (1981) An interpretation of trends in grain size measures. J Sediment Res 51:611–624

Mejjad N, Laissaoui A, El-Hammoumi O, Benmansour M, Benbrahim S, Bounouira H, Benkdad A, Bouthir FZ, Fekri A, Bounakhla M (2016) Sediment geochronology and geochemical behavior of major and rare earth elements in the Oualidia Lagoon in the western Morocco. J Radioanal Nucl Chem 309:1133–1143. https://doi.org/10.1007/s10967-016-4714-8

Nelson DW, Sommers LE (1996) Total carbon, organic carbon and organic matter. In: Sparks DL, Page AL, Helmke PA, Loeppert RH (eds) Methods of soil analysis part 3—chemical methods. ASA, SSSA, Inc., Madison, pp 961–1010

Pempkowiak J, Kulinski K (2012) Carbon cycling in the Baltic sea. Springer

Pimentel D (2006) Soil erosion: a food and environmental threat. Environ Dev Sustain 8:119–137. https://doi.org/10.1007/s10668-005-1262-8

Putyrskaya V, Klemt E, Rollin S, Astner M, Sahli H (2015) Dating of sediments from four Swiss prealpine lakes with ^{210}Pb determined by gamma-spectrometry: progress and problems. J Environ Radioact 145:78–94

Robbins JA (1978) Geochemical and geophysical applications of radioactive lead isotopes. In: Nriago JP (ed) Biogeochemistry of lead. North Holland, Elsevier, pp 285–393

Ruiz-Fernández AC, Frignani M, Hillaire-Marcel C et al (2009) Trace metals (Cd, Cu, Hg, and Pb) accumulation recorded in the intertidal mudflat sediments of three coastal Lagoons in the Gulf of California, Mexico. Estuaries Coasts 32:551–564. https://doi.org/10.1007/s12237-009-9150-3

Sanchez-Cabeza JA, Ruiz-Fernandez AC (2012) ^{210}Pb sediment radiochronology: an integrated formulation and classification of dating models. Geochim Cosmochim Acta 82:183–200

Sansone FJ, Spalding HL, Smith CM (2008) Oceanography: methods submersible-operated porewater sampler for permeable sediments. 119–125

Semertzidou P, Piliposian GT, Chiverrell RC, Appleby PG (2019) Long-term stability of records of fallout radionuclides in the sediments of Brotherswater, Cumbria (UK). J Paleolimnol 61:231–249

Sholkovitz ER (1983) The geochemistry of plutonium in fresh and marine water environments. Earth Sci Rev 19:95–161

Sun X, Fan D, Tian Y, Zheng S (2017) Normalization of excess ^{210}Pb with grain size in the sediment cores from the Yangtze River Estuary and adjacent areas: implications for sedimentary processes. Holocene 28:545–557. https://doi.org/10.1177/0959683617735591

Sundborg A, Calles B (2001) Water discharges determined from sediment distributions: a palaeohydrological method. Geogr Ann Ser B 83(1–2):39–54. https://doi.org/10.1111/j.0435-3676.2001.00143

Turner LJ, Delorme LD (1996) Assessment of Pb-210 data from Canadian lakes using the CIC and CRS models. Environ Geol 28:78–87. https://doi.org/10.1007/s002540050080

United States Department of Energy (USDOE) (1992) EML procedures manual, Report HASL 300

Van Hengstum PJ, Reinhardt EG, Boyce JI, Clark C (2007) Changing sedimentation patterns due to historical land-use change in Frenchman's Bay, Pickering, Canada: evidence from high-resolution textural analysis. J Paleolimnol 37(4):603–618. https://doi.org/10.1007/s10933-006-9057-y

Von Gunten L, Grosjean M, Beer J, Grob P, Morales A, Urrutia R (2009) Age modeling of young non-varved lake sediments: methods and limits. Examples from two lakes in Central Chile. J Paleolimnol 42:401–412

Voss M, Larsen B, Leivuori M, Vallius H (2000) Stable isotope signals of eutrophication in Baltic Sea sediments. J Marine Syst 25(3–4):287–298. https://doi.org/10.1016/S0924-7963(00)00022-1

Walling DE, Quine TA (1992) The use of caesium-137 measurement in soil erosion surveys, vol 210. IAHS publication, Wallingford, pp 143–152

Wan GJ, Chen JA, Wu FC, Xu SQ, Bai ZG, Wan EY, Wang CS, Huang RG, Yeager KM, Santschi PH (2005) Coupling between 210Pbex and organic matter in sediments of a nutrient-enriched lake: an example from Lake Chenghai, China. Chem Geol 224:223–236. https://doi.org/10.1016/j.chemgeo.2005.07.025

Weaver JC (1994) Sediment characteristics and sedimentation rates in Lake Michie, Durham County, North Carolina, 1990–92. Raleigh, N.C., U.S. Dept. of the Interior, U.S. Geological Survey

Xu M, Dong X, Yang X, Chen X, Zhang Q, Liu Q, Id RW, Yao M, Id TAD, Jeppesen E (2017) Recent sedimentation rates of shallow lakes in the middle and lower reaches of the Yangtze River. Patterns Control Factors Implic Lake Manag. https://doi.org/10.3390/w9080617